JOURNAL OF GEOPHYSICAL RESEARCH, VOL. 106, NO. B1, PAGES 447–461, JANUARY 10, 2001

Geomagnetic field behavior before and after the Kauai reverse-normal polarity transition

Scott W. Bogue

Department of Geology, Occidental College, Los Angeles, California

Abstract. New paleomagnetic results from 4 m.y. old lava flows from Kauai, Hawaii, suggest that strong poloidal field is associated with an unusual state of the geodynamo that follows attempts at polarity reversal (successful or not). The new data comprise 50 paleomagnetic sites from superposed lava flows occurring just below and above the Kauai reverse-normal polarity transition. A composite record of 45 distinct field determinations was constructed by combining sites that record similar ancient field and correlating them to previously published results from Kauai. Of the 45 data, 25 include paleointensity estimates derived from double-heating experiments. A comparison of the composite record from Kauai with two similar data sets from volcanic sequences shows that field variability (in direction, intensity, or both) can change substantially across a polarity transition. These changes, however, do not appear to be systematic in sign or magnitude. The only feature common to all three records is high field strength in the posttransitional interval, interpreted here as a transient phenomenon associated with the reversal process.

1. Introduction

There is general agreement that geomagnetic field intensity decreases by 80% to 90% during polarity reversals (see reviews of *Bogue and Merrill* [1992] and *Merrill and McFadden* [1999]). Unfortunately, other systematic features of transitional field behavior have proven difficult to resolve. Much debate in recent years has centered on the issue of whether lateral inhomogeneity in the lower mantle or core-mantle boundary controls the geometry of field reversal [*Clement*, 1991; *Laj et al.*, 1991]. The strongest evidence for this kind of field behavior comes from records of geomagnetic reversals preserved by Neogene sediments and sedimentary rocks [e.g., *Tric et al.*, 1991]. These records commonly exhibit virtual geomagnetic pole (VGP) paths that are longitudinally confined and preferentially located near 90°E or 270°E. It is well known, however, that geomagnetic reversals are associated with rapid field change (the entire process takes only a few thousand years) and field strength that is an order of magnitude lower than usual. Both conditions can adversely affect the fidelity of detrital remanence. Longitudinal confinement and preference of VGP paths is less apparent in volcanic reversal records [*Prévot and Camps*, 1993], but these data offer very incomplete sequences in time and (like the sedimentary records) are poorly distributed around the globe. Despite considerable effort by many paleomagnetists, this aspect of transitional field behavior remains controversial [*Merrill*, 1997; *Merrill and McFadden*, 1999].

The motivation for this study was the idea that systematic, reversal-related field behavior might occur before or after the main directional switch and associated intensity low. It seems plausible that field behavior of this sort, which we here term "epitransitional" might involve slower change and higher field strengths and thus be easier to document paleomagnetically. For example, computer simulations of the geodynamo suggest that reversals may initiate in two quite different ways, with reverse poloidal field propagating either outward from or inward toward the boundary between the inner and outer cores [*Glatzmaier and Roberts*, 1995; *Glatzmaier et al.*, 1999]. A question for paleomagnetists is whether either mechanism produces distinctive pretransitional field behavior at the surface, so that the two might be distinguished. A second possibility arises from the lack of very short polarity intervals in the geomagnetic polarity time scale, an observation implying that the geodynamo remains in an unusual state for several tens of thousands of years in the posttransitional interval [*McFadden and Merrill*, 1993]. Is there paleomagnetic evidence that the properties of the posttransitional geodynamo that inhibit reversals also produce distinctive field behavior at Earth's surface?

In this study, we examined the paleomagnetism of lava sequences that lie directly below and above the Kauai reverse-normal (R-N) transition [*Bogue and Coe*, 1984] looking for distinctive, epitransitional field behavior. The paleomagnetic record from the lavas comprises 25 distinct pretransitional data, 12 with paleointensity so that the full geomagnetic vector is documented, and 20 posttransitional data including 13 full vectorial determinations. The data show that substantial changes in field variability occur across the Kauai R-N polarity reversal. Similar results from two other detailed volcanic sequences, however, show that the sign and magnitude of the changes vary between reversals. The only distinctive field behavior displayed by all three records is high field strength following intervals when the field direction is transitional. Like *Bogue and Paul* [1993], we speculate that the strong poloidal field may be associated with conditions that inhibit reversals in the immediate posttransitional interval.

2. Geological Background and Sample Collection

The lava flows sampled for this study are part of the Napali Series of the Waimea Canyon Basalt [*Langenheim and Clague*, 1987] (Figure 1). This volcanic unit has traditionally been

Paper number 2000JB900319.
0148-0227/01/2000JB900319$09.00

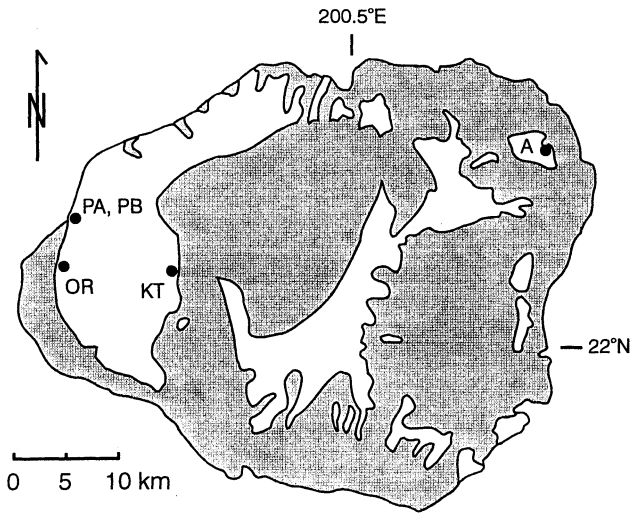

Figure 1. Location map and generalized geology, Kauai, Hawaii. Outcrop extent of Napali Series shown in white. Paleomagnetic sites mentioned in text are PA (Polihale A; 22.10°N; 200.26°E); PB (Polihale B; 22.10°N; 200.26°E); OR (Ohaiula Ridge; 22.07°N; 200.24°E); KT (Kukui Trail; 22.06°N; 200.35°E); and A (Anahola; 22.16°N; 200.67°E).

interpreted as the main shield building lavas of the Hawaiian island of Kauai [e.g., *MacDonald et al.*, 1960]. Recent work by *Holcomb et al.* [1997], however, suggests that Kauai may actually comprise at least two main shields. As discussed in more detail below, this new interpretation implies that the R-N polarity reversal boundary on eastern Kauai (the Anahola site of *Bogue and Coe* [1984]) may not correlate to the R-N boundary on western Kauai that was the target of this study.

Bogue and Coe [1982] located the Kauai R-N transition zone about 180 m above sea level on Polihale Ridge. In this vicinity, near Kauai's western extreme, lava flows of the Napali Series are accessible in excellent seacliff exposures. The transitional horizon is traceable from Polihale Ridge both northward, where its elevation increases to over 460 m, and southeastward toward the Mana town site where its elevation is ~60 m. Samples for this study were collected from the pretransitional lava flows at Polihale Ridge from sea level up to the lowest of the flows sampled by *Bogue and Coe* [1982] at an elevation of ~145 m. (We will refer to these newly collected flows as the Polihale B locality and to the directly overlying flows collected by *Bogue and Coe* [1984] as the Polihale A locality.) For detail on the posttransitional field we collected samples at Ohaiulu Ridge, ~4.5 km southeastward of Polihale Ridge. At this locality the transitional horizon is ~100 m above sea level, and good outcrop can be found all the way to ~240 m above sea level. As discussed by *Bogue and Paul* [1993], the Kauai R-N transition is likely one of three R-N transitions in Chron 3n (i.e., it formed between 4.62 Ma and 4.18 Ma according to timescale of *Cande and Kent* [1995]). The entire reversely magnetized section below the R-N horizon which *Bogue* [1982] inferred to be ~460 m thick near the sampling localities therefore spans between 90 and 190 kyr. Only 300 m of the normally magnetized section above the R-N transition is exposed [*Bogue*, 1982]; it likely spans between 90 and 140 kyr (timescale of *Cande and Kent* [1995]).

We used a gasoline-powered drill to collect five 2.5-cm-diameter core samples from each lava flow. The cores were oriented using a magnetic compass, with backsights to distant landmarks to correct for local variations (never more than a few degrees) in the magnetic declination. Many of the lava flows we sampled had complex internal structure (e.g., multiple vesicular or reddish rubbly zones), and it was difficult to identify with certainty the boundaries between distinct cooling units. As the paleomagnetic results show, we tended to oversample, and in many cases, successive paleomagnetic sites likely represent a single cooling unit.

3. Experimental Procedure

3.1. Directional Measurements

The natural remanent magnetizations (NRMs) of 2.5-cm-long specimens from each oriented core were measured on a Molspin rock magnetometer. On the basis of our previous experience with the paleomagnetism of lava flows from this locality [*Bogue and Coe*, 1982], we anticipated that the remanence of most samples would comprise an original thermoremanent magnetization (TRM) and minor secondary components of lightning-induced isothermal remanent magnetization (IRM) or Brunhes age viscous remanent magnetization (VRM). For sites where the NRM directions of the five samples were tightly clustered, we typically subjected the samples to light alternating field (AF) demagnetization with peak fields of 10 to 20 mT to make sure that minor secondary components were removed. For some sites, especially those near the top of the seacliffs at Ohaiula Ridge, the NRM directions were scattered presumably because the outcrops there were more exposed to lightning strikes. For sites of this kind, blanket application of higher levels of AF demagnetization (40 mT in the worst cases) were used to minimize secondary components of magnetization. As demonstrated by the detailed thermal demagnetizations from the paleointensity experiments, the magnetic behavior of these samples is straightforward, and so detailed AF demagnetization experiments and principal component analysis would not produce significantly better estimates of the site-mean directions or errors.

3.2. Paleointensity Experiments

The paleointensity experiment used for this study is a variation on the method of *Coe* [1967], which in turn is derived from the procedure of *Thellier and Thellier* [1959]. Like *Coe* [1967] we conducted paired heatings to a series of increasingly higher temperatures. Unlike *Coe* [1967], however, we (1) aligned each sample in the furnace so that its initial NRM direction was ~90° to the field applied in the furnace, (2) conducted the first heating at each temperature with a 35 μT axial field in the furnace (the "field-on" heating) and the second heating with the field off, the opposite of the usual procedure, and (3) had the field on during the field-off heating until 5 to 10 min before the peak temperature was reached. The point of this procedure was to make obvious any component of magnetization acquired by the sample that was not removed by thermal demagnetization at the same temperature. Because each sample experienced the first heating, first cooling, and (most of) the second heating cycle with the field on in the furnace, such a component would likely form parallel to the laboratory field rather than in zero field (during the second cooling). On the basis of previous experience with samples from Kauai, we were anticipating high blocking temperature (T_b) remanence components produced by new magnetic mineral growth (e.g., magnetite produced by disproportionation of cation-deficient titanomagnetite), a form of

chemical remanent magnetization. Although these anomalous components could have other origins, we will we refer to them as CRMs throughout this paper.

Almost all samples showed evidence of CRM growth at some stage during the experiments, but we avoided using data from temperatures above which the CRM was greater than ~15% of the NRM remaining in the sample. Furthermore, we vectorially subtracted any CRM component before calculating the paleointensity from the remanence measurements. A few samples were misoriented in the furnace with their NRM aligned close to the laboratory field direction, precluding the analysis for CRM acquisition. Only one such sample (core 179 from flow OR14) eventually yielded an acceptable paleointensity.

Remanence measurements were performed on either a Molspin or Schonstedt fluxgate spinner magnetometer. Because the moment calibration of the Molspin could drift significantly during a measurement session, we measured a calibration standard (containing magnetic recording tape) before each sample measurement during the paleointensity experiments. Appendix A provides a description of the controlled-field furnace used in the experiments, our sample selection procedure, and details on the analysis of the paleointensity results.

4. Results

4.1 Directions

Tables 1 and 2 show the results of the directional measurements. Table 1 lists the site-mean remanence and associated statistics for every sampled horizon, not all of which represent distinct cooling units. Unless paleointensity data suggested otherwise, we assumed that successive paleomagnetic sites with very similar directions (within ~5°) were part of a single cooling unit or from separate flows erupted in quick succession (<100 years, based on recent secular variation (SV) in Hawaii [see *Holcomb et al.*, 1986]. Either way, these sites probably do not represent independent samplings of the ancient field and so have been combined (using unit-weighted sample directions) to form the "vector groups" listed in the Table 2. Sites yielding paleointensity estimates were combined only if the directions were similar and the paleointensities differed by <10%. For various reasons (e.g., because of extended intervals when the SV was zero; because the field strength may have varied even though its direction did not), the data may represent more independent samplings of the field than shown in Table 2. Of the 30 vector groups from Polihale B and Ohaiula Ridge, 19 consist of single paleomagnetic sites. The average precision parameter k for the vector groups is 656 and the average α_{95} is 3.3°, so these mean directions are very precisely determined.

Table 2 also presents an inferred stratigraphy of pretransitional section at Polihale B, the posttransitional section at Ohaiula Ridge and the R-N transition localities at Polihale A and Kukui Trail [*Bogue and Coe*, 1984]. The highest flow of Polihale B lies directly under the lowest flow of Polihale A; their stratigraphic relation is unequivocal. As described above, the R-N transition can be traced from the Polihale Ridge to Ohaiula Ridge, and there is no question that the highest flows at the Polihale locality and lowest flows at the Ohaiula Ridge locality are equivalent stratigraphically. The correlation between the R-N transitions at Polihale and Kukui Trail localities (~11 km apart) is also secure. Recently published geochemical evidence [*Holcomb et al.*, 1997], however, casts doubt on the correlation of these localities (all on western Kauai) with the Anahola locality of *Bogue and Coe* [1984], which lies on the opposite side of the island. It now seems likely that Napali Series lavas on western and eastern Kauai originated from separate, geochemically distinct magma chambers. Although it is possible these two sources were active at the same time, it is more likely that the Napali flows exposed on western Kauai and at Anahola accumulated during different R-N reversals. We have excluded results from flows at the Anahola locality from this study but

Table 1. Paleomagnetic Directions From Sampled Units[a]

Flow	D, deg	I, deg	N_d	k	α_{95}, deg	Lon, °E	Lat, °N
OR28	346.9	37.4	5	321	4.3	126.1	77.5
OR27	356.1	41.0	5	392	3.9	166.7	84.2
OR26	009.8	41.1	5	2664	1.5	266.7	79.8
OR25	342.3	44.2	5	379	3.9	141.2	72.3
OR24	341.4	41.1	5	560	3.2	133.0	72.1
OR23	329.6	18.4	5	264	4.7	101.3	59.1
OR22	335.4	16.0	5	454	3.6	093.9	63.8
OR21	338.1	16.0	4	53.6	12.7	090.9	66.2
OR20	332.0	19.7	5	886	2.6	100.9	61.5
OR19	333.9	17.8	5	2367	1.6	097.3	62.9
OR18	335.6	19.0	5	235.6	5.0	097.1	64.7
OR17	337.2	06.9	5	395	3.9	082.9	62.8
OR16	352.3	24.6	5	194	5.5	076.6	80.4
OR15	352.5	30.5	5	585	3.2	096.3	82.4
OR14	352.1	27.9	5	1382	2.1	087.3	81.4
OR13	350.3	30.3	5	1872	1.8	100.2	80.4
OR12	349.5	28.6	5	1375	2.1	096.1	79.3
OR11	352.1	27.1	5	717	2.9	084.6	81.1
OR10	351.4	31.2	5	336	4.2	101.6	81.5
OR9	351.9	31.6	5	677	2.9	102.4	82.1
OR8	353.2	29.3	5	1957	1.7	088.9	82.7
OR7	354.6	27.7	5	1317	2.1	076.1	83.3
OR6	353.7	28.1	5	920	2.5	082.0	82.7
OR5	003.8	28.7	5	227	5.1	339.9	84.8
OR4	001.2	27.1	5	2240	1.6	010.9	85.2
OR3	004.3	38.5	5	438	3.7	260.6	85.2
OR2	353.0	38.8	5	367	4.0	140.1	82.8
OR1	002.5	38.0	5	310	4.4	249.7	86.7
PB22	173.5	-51.3	5	376	4.0	002.0	-75.8
PB21	175.4	-47.7	5	485	3.5	002.6	-79.3
PB20	187.1	-39.0	5	196	5.5	089.2	-82.7
PB19	165.0	-10.6	5	392	3.9	253.9	-70.0
PB18	163.8	-11.9	5	675	2.9	257.6	-69.6
PB17	184.9	-47.0	5	452	3.6	050.1	-79.8
PB16	183.1	-47.8	5	941	2.5	040.4	-79.7
PB15	165.7	-27.3	5	245	4.9	278.9	-75.6
PB14	172.7	-25.0	5	416	3.8	256.1	-80.9
PB13	160.0	-45.1	5	822	2.7	321.2	-70.1
PB12	147.7	-50.8	5	2086	1.7	324.7	-58.4
PB11	140.3	-50.5	5	303	4.4	321.8	-52.3
PB10	145.6	-52.9	5	973	2.5	327.3	-56.1
PB9	165.4	-20.4	5	25	15.5	266.1	-73.6
PB8	163.2	-25.8	5	646	3.0	279.0	-73.0
PB7	159.5	-26.6	5	515	3.4	284.0	-69.8
PB6	154.4	-22.3	5	1097	2.3	282.0	-64.3
PB5	164.7	-08.1	5	215	5.2	251.9	-68.9
PB4	206.7	-26.5	5	157	6.1	122.0	-63.9
PB3	159.8	-19.5	5	249	4.9	273.2	-68.5
PB2	177.5	-33.1	5	542	3.3	273.6	-87.4
PB1	177.2	-25.9	5	360	4.0	232.1	-84.0

[a]Flow names beginning with OR are from Ohaiula Ridge; those beginning with PB are from Polihale Ridge. Order is from old (at bottom) to young (at top). D is the eastward declination and I the downward inclination. N_d is the number of sample directions used to calculate the flow-mean direction. The k and α_{95} are precision parameter and 95% confidence cone of *Fisher* [1953]. Lon and Lat are the longitude and latitude of the VGP calculated for a site at the Hawaiian hotspot (205°E, 19°N).

Table 2. Inferred Stratigraphy, Vector Group Remanence Direction, and Vector Group Paleointensity of Sampled Units[a]

VG	Flows	D, deg	I, deg	N_d	k	α_{95}, deg	F_{anc}, (μT)	N_f	Percent +(-)	Lon, °E	Lat, °N	VDM, (x10^{22} A m^2)
45	OR28	346.9	37.4	5	321	4.3				126.1	77.5	
44	OR27	356.1	41.0	5	392	3.9	49.9±1.7	4	6.4(7.2)	166.7	84.2	10.6
43	OR26	009.8	41.1	5	2664	1.5				266.7	79.8	
42	OR24-25	341.9	42.6	10	420	2.4				137.0	72.3	
41	OR18-23(22)	335.4	16.0	5	454	3.6	35.8±3.5	4	27.1(17.9)	93.9	63.8	9.0
40	OR17	337.2	06.9	5	395	3.9				82.9	62.8	
39	OR16	352.3	24.6	5	194	5.5				76.6	80.4	
38	OR14-15	352.3	29.2	10	721	1.8	48.1±3.6	4	8.9(12.7)	91.4	81.9	11.3
37	OR13	350.3	30.3	5	1872	1.8	44.7±3.3	3	17.2(4.9)	100.2	80.4	10.4
36	OR10-12	351.0	28.9	15	481	1.7	50.4±1.4	10	17.5(12.5)	93.8	80.7	11.8
35	OR6-9(7)	354.6	27.7	5	1317	2.1	31.1±0.3	4	1.3(2.3)	76.1	83.3	7.4
34	OR4-5(4)	001.2	27.1	5	2240	1.6	48.1±2.0	3	7.5(6.7)	10.9	85.2	11.4
33	OR3	004.3	38.5	5	438	3.7	66.6±0.6	3	0.9(1.7)	260.6	85.2	14.5
32	OR2	353.0	38.8	5	367	4.0	53.6±2.1	2	3.4(4.5)	140.1	82.8	11.6
31	OR1	002.5	38.0	5	310	4.4	60.4±2.5	3	7.1(5.8)	249.7	86.7	13.2
30	KT30-32(30,32)	000.9	32.7	13	1790	1.0	44.4±0.2	4	0.9(0.9)	349.5	88.5	10.1
29	PA12-13(12)	355.0	46.3	8	1531	1.4	41.2±2.3	3	10.9(6.8)	177.9	80.2	8.3
28	PA11	357.2	25.3	3	624	4.9				50.7	83.7	
27	KT28-29	013.4	24.6	13	618	1.7	37.5±0.8	6	5.6(8.8)	318.4	75.8	9.1
26	PA10	014.3	34.0	9	1300	1.4				294.2	76.5	
25	KT25-26(26)	192.3	-16.6	7	364	3.2	29.3±2.1	4	22.5(5.8)	154.7	-74.1	7.3
24	KT19-24(23)	191.0	-20.4	7	159	4.8	21.8±1.4	3	13.8(6.0)	152.0	-76.4	5.4
23	KT16-18(18)	163.6	-29.8	6	468	3.1	29.2±2.2	3	14.0(11.3)	286.6	-74.1	6.8
22	KT15	005.4	42.4	7	487	2.7				246.2	82.5	
21	KT10-14(13)	158.9	-30.0	7	2504	1.2	30.1±0.4	3	3.3(1.0)	290.1	-69.7	7.0
20	KT8-9(9)	158.1	-27.7	7	191	4.4	43.1±4.6	2	15.1(2.1)	286.8	-68.6	10.2
19	KT5-7(5)	170.3	-40.3	7	3031	1.1	34.8±5.2	3	36.8(1.1)	320.4	-80.1	7.5
18	PA7-9	161.6	-45.6	22	291	1.8				323.8	-71.3	
17	KT1-4,PA2-6(PA3)	170.1	-47.3	6	2054	1.5				343.1	-76.9	
16	PA1	184.1	-50.7	7	218	4.1				40.8	-77.0	
15	PB21-22	174.5	-49.5	10	370	2.5				2.3	-77.6	
14	PB20	187.1	-39.0	5	196	5.5				89.2	-82.7	
13	PB18-19	163.8	-11.9	5	675	2.9	42.4±1.6	3	3.8(8.5)	257.6	-69.6	10.8
12	PB16-17	184.0	-47.4	10	646	1.9	59.5±2.2	3	3.0(8.7)	45.2	-79.8	11.9
11	PB15	165.7	-27.3	5	245	4.9				278.9	-75.6	
10	PB14	172.7	-25.0	5	416	3.8				256.1	-80.9	
9	PB13	160.0	-45.1	5	822	2.7				321.2	-70.1	
8	PB10-12	144.5	-51.5	15	459	1.8	42.5±1.4	4	4.7(7.5)	324.6	-55.6	8.1
7	PB7-9	160.0	-26.2	9	645	2.0	30.4±2.9	3	16.4(10.9)	282.9	-70.1	7.3
6	PB6	154.4	-22.3	5	1097	2.3				282.0	-64.3	
5	PB5	164.7	-08.1	5	215	5.2	17.8±0.4	3	4.5(3.4)	251.9	-68.9	4.6
4	PB4	206.7	-26.5	5	157	6.1				122.0	-63.9	
3	PB3	159.8	-19.5	5	249	4.9				273.2	-68.5	
2	PB2	177.5	-33.1	5	542	3.3				273.6	-87.4	
1	PB1	177.2	-25.9	5	360	4.0	37.1±1.1	3	4.9(5.1)	232.1	-84.0	8.9

[a]VG is the vector group number. Order is from old (at bottom) to young (at top). Flow names beginning with KT and PA are previously collected sites from Kukui Trail and Polihale Ridge (*Bogue and Coe*, [1984]). Flows are those that constitute each vector group. For vector groups yielding a paleointensity (and VG17), only the sites shown in parentheses (the ones contributing paleointensity data) were used to calculate the vector group direction. N_d is the number of sample results averaged for vector group direction. F_{anc} is ancient field intensity. N_f is the number of sample results used to calculate vector group paleointensity. Percent +(-)is the full range of sample paleointensities above and below the vector group mean. VDM is the virtual dipole moment (for a site at 205°E, 19°N). Other abbreviations are as in Table 1.

emphasize that none of our conclusions are significantly affected by this choice.

The sequence of vector groups near the R-N transition mostly follows the correlations of *Bogue and Coe* [1984], with some additional grouping of sites, minor reordering of Polihale and Kukui Trail sites below the R-N horizon, and omission of the data from the Anahola locality on eastern Kauai. *Bogue and Coe* [1984] considered the field behavior recorded by the flows now in vector groups 23 through 25 to be transitional. This interpretation was based primarily on the low paleointensities from flows at the Anahola locality that appeared (based on paleomagnetic directions) to correlate between VG23 and VG24. Additional evidence for the interpretation came from VG22, a single flow at the Kukui Trail whose normal-like direction suggested that complex, possibly rapid field change was occurring. Without the Anahola data, however, it seems most reasonable to consider all the field behavior recorded by flows below the R-N horizon to be pretransitional in character; that is, occurring before the intensity drop and directional change associated with the main reversal in direction at the Earth's surface. Identical remanence directions from the flows in VG17 provide a tie point between the Polihale and Kukui Trail localities. The inferred stratigraphic order of the highest flows at the Polihale and Kukui Trail localities (now VG37 and VG38) is the opposite of that listed by *Bogue and Coe* [1984], a change that produces a smoother variation in ancient field intensity. We follow *Bogue and Paul* [1993] in interpreting the lowest flows at Ohaiula Ridge as stratigraphically atop the highest flows at Kukui Trail, even though alternative correlations are equally plausible [*Bogue and Paul*, 1993].

The directional changes of the field before and after reversing

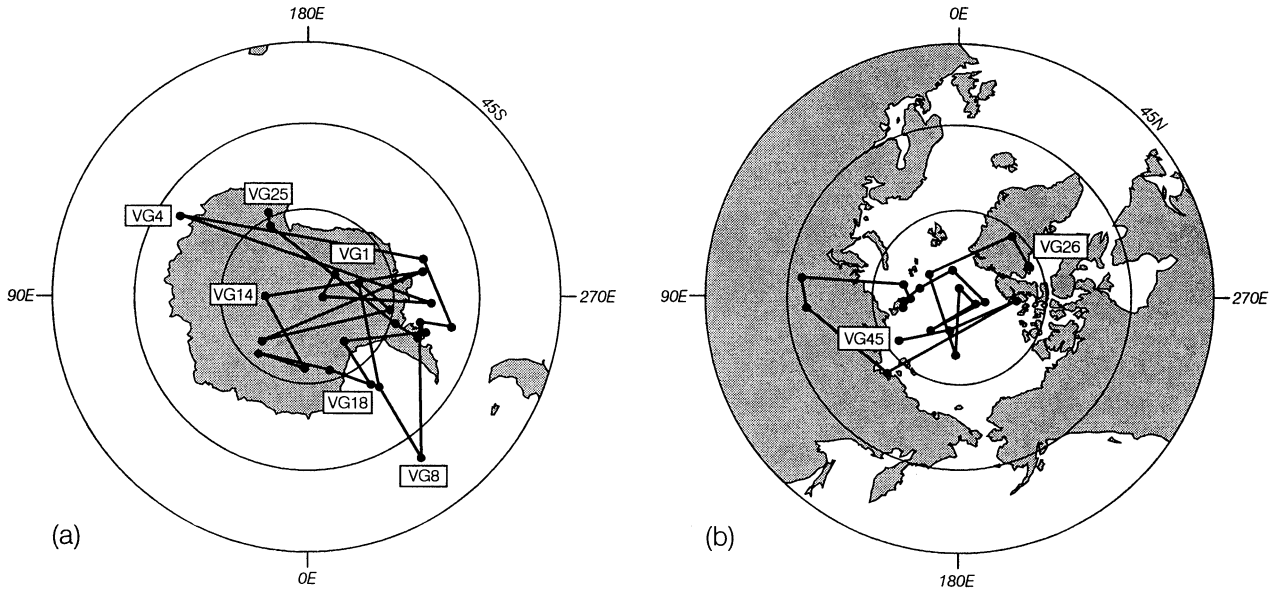

Figure 2. Equal area plots (polar views to latitude 45°) of VGP sequences (a) before and (b) after the Kauai R-N transition. VG22 is omitted.

are shown in Figure 2, where the data are plotted as virtual geomagnetic poles (VGPs). In the pretransitional sequence the VGP begins near the South Pole and then undergoes large (>15°) swings to the western (four times) and eastern hemispheres. Less than half the vector groups lie within 15° of the spin axis. As described in more detail below, the second swing into the western hemisphere (defined by vector groups 5 through 11) is associated with low field intensity and is followed by unusually high field intensity (in VG12). In the posttransitional sequence, all but three of the 20 VGPs lie within 15° of the spin axis and some are associated with unusually high paleointensities [*Bogue and Paul*, 1993]. Toward the end of the sequence, vector groups 40 through 42 record a substantial move of the VGP away from the spin axis into the eastern hemisphere.

It is apparent in Figure 2 that the secular variation of the field (as expressed by its directional change) was greater before the reversal than after. This aspect of field behavior is best described by the angular standard deviation (S) of unit-weighted VGPs from the spin axis [*McFadden et al.*, 1988] after a slight correction for motion of the Pacific plate relative to hotspots (pole of Engebretson et al. [1985]). For the pretransitional interval, S=18.6° (not including the anomalous direction of VG22). For the posttransitional interval, S=12.9°, a value that differs from the preliminary calculation of *Bogue and Paul* [1993] by 0.5° and is approximately two thirds the pretransitional value. As discussed below, a nearly identical decrease in S accompanied the R-N reversal at 15 Ma recorded by the lavas at Steens Mountain [*Mankinen et al.*, 1985].

4.2 Paleointensities

Table 3 summarizes the results for all samples that yielded a paleointensity, and Figures 3 through 7 show NRM-TRM diagrams [*Arai*, 1963] and associated plots representing typical sample behaviors. Sample 6W144 is an example of the samples

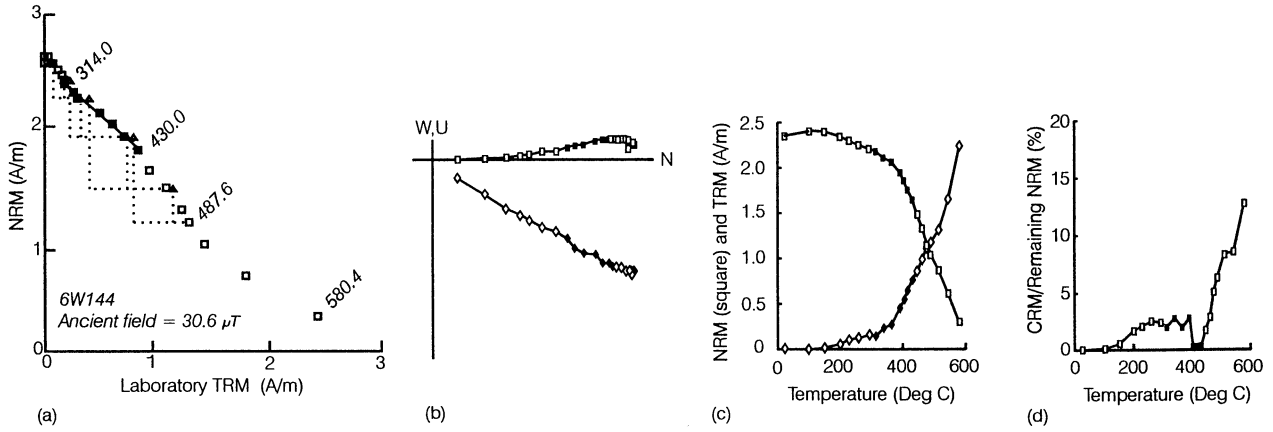

Figure 3. Graphs showing behavior of sample 6W144 in the paleointensity experiment. (a) NRM-TRM diagram. (b) Orthogonal vector endpoint diagram showing remanence after field-off heatings. Vector endpoints projected to horizontal plane shown with squares; endpoints projected to north-up plane shown with diamonds. (c) NRM (squares) remaining after heating in zero field and TRM (diamonds) acquired after heating to same temperature in 35 μT field. (d) Apparent CRM (as percentage of ideal NRM remaining) after field-off step to indicated temperature. Solid symbols on the graphs indicate data from blocking temperature interval used to calculate the sample paleointensity. In Figure 3a, triangles indicate PTRM checks (see text for explanation).

Table 3. Paleointensity Experiments Summary[a]

VG	Flow	Sample	F_{anc}, μT	q	f, %	$-s_b/b$, %	g	n	CRM, %	Start T, °C	End T, °C
44	OR27	241	46.3±1.2	6.4	60.4	2.6	0.852	12	10	99.7	426.3
44	OR27	242	47.2±0.9	7.5	51.9	1.9	0.841	11	8	77.2	413.8
44	OR27	243	53.1±0.7	11.7	54.0	1.4	0.858	10	6	149.6	412.6
44	OR27	244	51.7±2.1	2.9	40.4	4.1	0.836	10	15	95.3	377.3
41	OR22	216	29.4±1.3	2.2	25.9	4.4	0.822	7	15	374.5	477.0
41	OR22	217	33.5±1.2	3.0	30.0	3.7	0.812	7	14	373.6	476.1
41	OR22	219	45.5±1.6	2.8	29.6	3.4	0.858	9	8	323.5	472.8
41	OR22	220	32.5±1.8	2.0	34.2	5.6	0.844	9	14	323.3	477.2
38	OR15	181	50.0±1.3	6.1	43.3	2.6	0.809	7	8	364.9	459.8
38	OR15	185	46.8±1.8	3.9	35.9	3.9	0.729	5	16	348.1	428.8
38	OR14	178	52.6±1.9	3.1	26.4	3.6	0.731	5	4	331.5	419.2
38	OR14	179	42.0±1.2	3.3	23.8	3.0	0.719	5	8	324.4	418.2
37	OR13	173	52.4±2.9	2.0	30.2	5.6	0.820	7	7	423.1	519.1
37	OR13	174	43.8±1.0	7.2	60.8	2.3	0.908	13	10	301.7	528.9
37	OR13	175	42.5±1.5	3.9	44.5	3.6	0.882	10	14	350.6	505.8
36	OR12	166	50.0±2.4	1.6	25.6	4.8	0.799	9	4	199.3	414.7
36	OR12	167	50.2±2.4	1.6	26.0	4.7	0.791	9	2	199.5	414.7
36	OR12	168	48.7±1.8	2.1	29.4	3.8	0.838	12	1	99.8	429.2
36	OR12	170	49.4±2.6	1.5	24.8	5.3	0.852	9	2	296.6	457.4
36	OR11	161	44.1±0.6	12.2	64.3	1.4	0.868	13	9	325.7	549.0
36	OR11	163	54.0±2.0	2.0	29.4	3.6	0.895	14	3	150.2	477.2
36	OR11	164	55.9±2.8	2.8	21.2	5.1	0.866	10	3	297.4	476.5
36	OR11	165	59.2±1.3	6.7	74.5	2.2	0.834	20	13	24.0	560.2
36	OR10	157	51.1±1.6	4.2	42.0	3.1	0.861	10	6	374.3	525.8
36	OR10	159	49.4±1.7	2.0	18.4	3.4	0.825	7	3	402.1	489.4
35	OR7	141	31.5±0.4	8.9	23.4	1.1	0.748	5	15	410.6	470.4
35	OR7	143	31.0±0.5	8.3	34.9	1.6	0.764	6	15	399.2	476.1
35	OR7	144	30.6±1.0	2.6	23.3	3.3	0.821	7	0	314.0	430.0
35	OR7	145	30.4±1.3	1.9	25.3	4.2	0.839	9	1	268.5	443.8
34	OR4	126	49.0±1.0	8.5	56.0	2.0	0.810	9	5	263.3	442.2
34	OR4	128	51.7±2.0	3.2	40.6	4.0	0.839	9	16	230.7	418.7
34	OR4	130	44.9±1.2	5.8	39.9	2.6	0.764	6	8	297.7	412.9
33	OR3	122	67.2±2.5	3.1	35.8	3.7	0.854	9	15	232.0	427.6
33	OR3	123	66.9±3.3	2.2	32.9	5.0	0.830	8	16	24.0	322.5
33	OR3	124	65.5±2.4	2.6	23.0	3.7	0.735	5	15	309.5	402.9
32	OR2	116	55.4±1.2	7.2	50.5	2.2	0.876	10	15	293.3	462.5
32	OR2	117	51.2±1.2	5.6	37.2	2.4	0.800	7	15	293.4	418.6
31	OR1	111	58.1±3.3	1.9	31.0	5.7	0.840	8	12	24.0	322.5
31	OR1	112	64.7±1.6	4.9	48.3	2.5	0.907	15	3	24.0	429.4
31	OR1	113	56.9±1.6	4.8	40.8	2.9	0.825	8	12	202.1	399.2
29	PA12	012	39.5±2.0	1.7	19.3	5.0	0.741	5	6	379.6	457.3
29	PA12	013	45.7±1.3	3.1	19.6	2.9	0.658	4	9	359.9	417.6
29	PA12	014	38.4±1.0	4.1	26.0	2.7	0.739	5	6	343.8	421.8
17	PA3	076	31.6±1.2	4.3	41.1	3.9	0.711	5	15	445.7	526.5
17	PA3	080	46.3±1.7	2.6	19.9	3.6	0.667	4	16	420.1	478.8
13	PB18	062	44.0±2.5	1.9	22.6	5.7	0.656	4	b	326.0	401.6
13	PB18	064	42.4±1.1	6.2	52.9	2.6	0.856	10	6	201.9	430.0
13	PB18	065	38.8±3.0	0.8	14.9	7.6	0.771	6	1	100.4	297.8
12	PB17	086	54.3±1.7	2.6	18.9	3.1	0.748	5	14	376.2	445.2
12	PB17	090	61.3±1.3	6.8	40.0	2.1	0.798	7	17	266.8	416.5
12	PB16	056	59.7±1.5	3.8	24.4	2.5	0.781	6	12	370.7	451.2
8	PB12	047	42.9±3.5	0.8	17.5	8.2	0.720	6	6	226.5	364.2
8	PB11	102	39.3±3.9	0.8	19.0	9.9	0.727	5	10	149.2	294.1
8	PB11	103	39.7±2.2	1.5	24.2	5.7	0.800	7	16	233.4	402.4
8	PB10	045	44.5±1.8	3.4	41.7	4.1	0.833	8	12	200.5	402.5
7	PB9	038	27.1±0.5	7.1	34.0	1.9	0.693	5	21	318.3	400.5
7	PB7	106	35.4±1.0	3.3	20.3	2.7	0.613	4	7	318.5	397.7
7	PB7	108	34.2±1.4	1.7	22.7	4.2	0.832	9	7	289.8	447.2
5	PB5	022	18.6±0.7	2.6	25.2	3.7	0.752	6	10	349.2	442.1
5	PB5	023	17.5±0.5	2.8	25.8	3.1	0.772	7	11	299.6	428.7
5	PB5	024	17.2±0.6	1.6	12.4	3.6	0.637	4	17	347.7	413.4
1	PB1	002	38.9±2.1	1.7	22.2	5.5	0.738	5	6	339.8	418.0
1	PB1	004	38.1±1.6	3.4	49.3	4.1	0.856	11	16	202.2	429.7
1	PB1	005	35.2±1.5	3.6	48.1	4.2	0.846	9	5	296.3	454.0

[a]Order is from old (at bottom) to young (at top). The q, f, s_b/b, g, and n are the quality factor, NRM fraction, slope uncertainty, gap factor, and number of NRM-TRM points used for the paleointensity estimate (all after *Coe et al.*, [1978]). The CRM is the size of the apparent CRM compared to the remaining NRM at the highest temperature NRM-TRM point used in the paleointensity estimate. Start T and end T are the temperatures of the first and last NRM-TRM points used to estimate the paleointensity. Other abbreviations are as in Tables 1 and 2.

[b]Sample improperly oriented in furnace so that CRM component could not be determined.

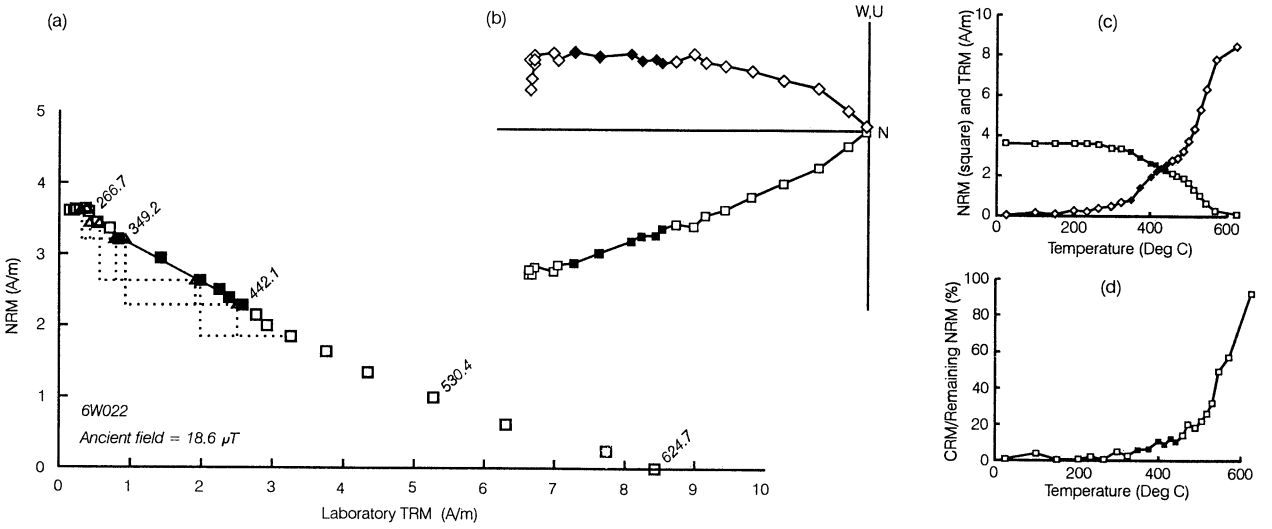

Figure 4. Behavior of sample 6W022 in the paleointensity experiment. (a) NRM-TRM diagram. (b) Orthogonal vector endpoint diagram (squares (diamonds) show the data projected to the horizontal (north-up) plane). (c) NRM (squares) and TRM (diamonds) versus temperature. (d) Apparent CRM versus temperature. Solid symbols on the graphs indicate data from blocking temperature interval used to calculate the sample paleointensity. See Figure 3 for fuller explanations of the plots.

that performed best in the experiments. The NRM-TRM diagram for sample 6W144 (Figure 3) shows a linear segment typical in extent for the samples, spanning 23% of the sample's NRM and 116° of the T_b distribution. Checks of TRM acquisition at lower T after heating to higher T (the "PTRM check" of *Coe et al.* [1978]) show evidence of only slight increases in TRM capacity. Plots of NRM and TRM versus T are simple in form, and the orthogonal vector diagram shows that the sample's NRM decayed linearly to the origin as it was thermally demagnetized. The plot of CRM/NRM versus temperature expresses this aspect of the experiment in a different way. The apparent CRM (i.e., component parallel to the laboratory field appearing in the NRM; see Appendix A) does not exceed the 5% of the remaining NRM in the sample until the sample is heated to nearly 500°C (well beyond the T_b interval used for the paleointensity estimate). We consider the paleointensity from this kind of sample to be very reliable.

Samples 6W022 and 6W013 show more complicated behavior than 6W144. Figure 4 shows that 6W022 had a linear NRM-TRM segment of typical length with excellent PTRM checks. The forms of the NRM and TRM versus T plots are more complicated than for 6W144 (Figure 3), with slight inflections indicative of two peaks in the T_b distribution. The orthogonal vector diagram and CRM plot show evidence of undesirable thermochemical alteration at temperatures lower than observed for 6W144, although the CRM component becomes a significant fraction of the sample's remanence only after most the NRM has been thermally demagnetized. Nevertheless, the CRM component reaches 10% of the NRM present in the sample at the highest-temperature point used in the paleointensity estimate (442°C), comparable to the magnitude of CRM at 580°C for 6W144. Sample 9Q013 (Figure 5) also has very good PTRM checks and moderate CRM acquisition but in addition shows a puzzling behavior during paired heating steps up to about 300°C. As can be seen in the NRM-TRM diagram and the plot of NRM and TRM versus T, there is a substantial decrease in NRM but very little TRM acquisition over this temperature interval. Excellent

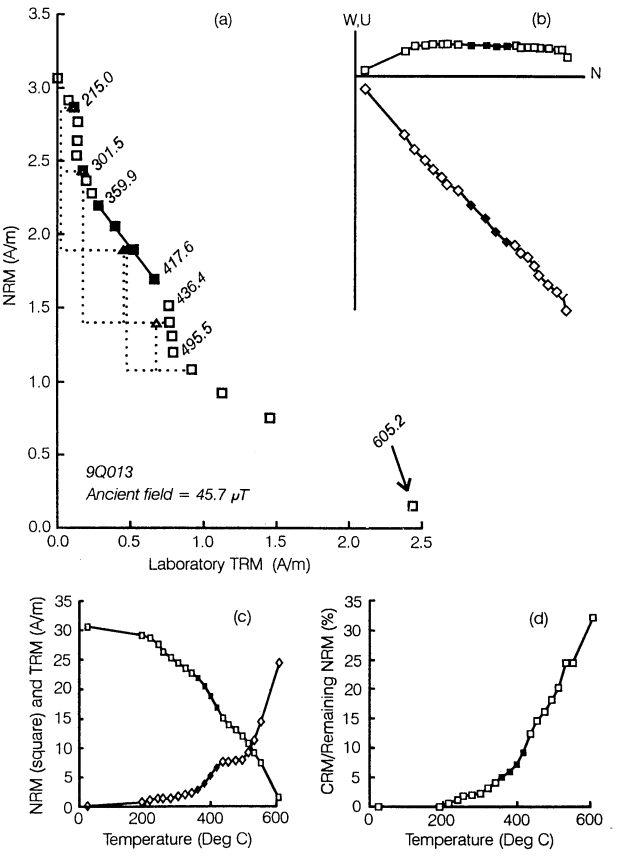

Figure 5. Behavior of sample 6W013 in the paleointensity experiment. (a) NRM-TRM diagram. (b) Orthogonal vector endpoint diagram (squares (diamonds) show the data projected to the horizontal (north-up) plane). (c) NRM (squares) and TRM (diamonds) versus temperature. (d) Apparent CRM versus temperature. Solid symbols on the graphs indicate data from blocking temperature interval used to calculate the sample paleointensity. See Figure 3 for fuller explanations of the plots.

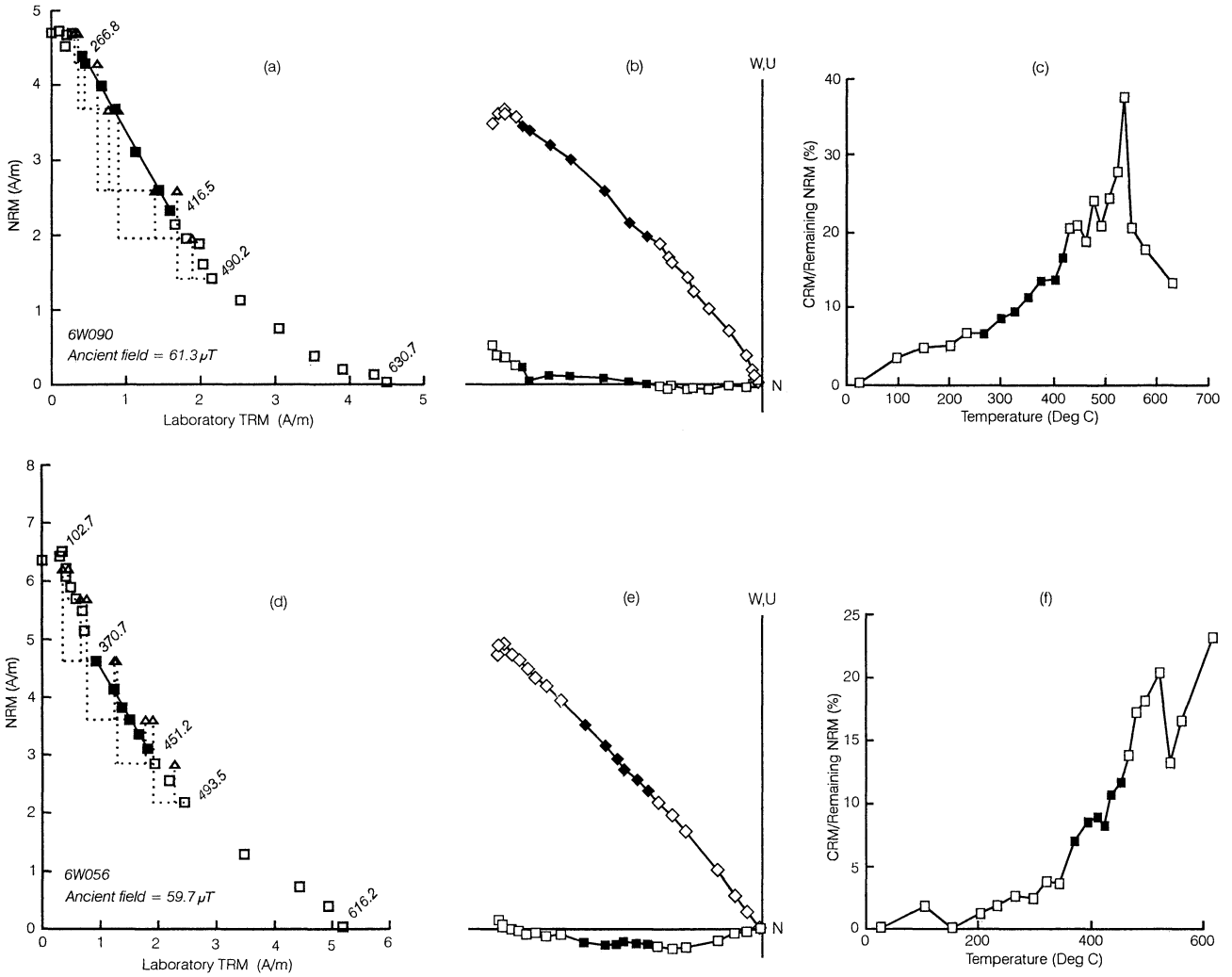

Figure 6. Behavior of two pretransitional samples (vector group 12) yielding high paleointensities. (a and d) NRM-TRM diagrams. (b and e) Orthogonal vector endpoint diagrams. (c and f) CRM acquisition plots. On Figures 6b and 6e, squares (diamonds) show the data projected to the horizontal (north-up) plane. Solid symbols on the graphs indicate data from blocking temperature interval used to calculate the sample paleointensity. See Figure 3 for fuller explanations of the plots.

PTRM checks back to 215°C and 302°C demonstrate that the drop is reproducible. Similar behavior was noted in Mesozoic basalts by *Kosterov and Prévot* [1998]. We do not fully understand the cause of this behavior but accept the paleointensity because so many other aspects of experiment appear normal.

Samples 6W090 and 6W056 (Figure 6) are from a pretransitional vector group that records unusually strong ancient field. The first of the two samples is relatively straightforward; the PTRM checks are excellent and the CRM growth is modest until well beyond the T_b interval from which the paleointensity was derived. The paleointensity for the second sample derives from a much shorter fraction of the NRM than the first. In addition, the PTRM checks show evidence that the TRM capacity of the sample was increasing during the laboratory heatings. The CRM component for 6W056, however, remained <10% of the remaining NRM until heated above 422°, about 100°C higher than the temperature at which CRM attained a comparable magnitude in 6W090. Despite these somewhat different behaviors, the two samples yield the same paleointensity.

Figure 7 shows examples of samples that experienced episodes of laboratory TRM loss as the temperature of the field-on heatings increased. This behavior results in a segment of the NRM-TRM curve that "hooks" (i.e., assumes positive slope) and has been described for other rock types [e.g., *Prévot et al.*, 1983]. Sample 6W126 (from vector group 34) exhibits a very large hook that occurs at temperatures just above these corresponding to a long linear segment on the NRM-TRM diagram. The very good PTRM checks back from a point within the linear segment suggest that the alteration producing the hook did not spoil the paleointensity estimate. The magnitude of the apparent CRM in this sample remained low until the sample was heated to near 600°C, so the loss in TRM capacity was probably not related to the growth of a new, high T_b magnetic phase. Sample 6W128 (from the same flow as 6W126) exhibits a much smaller hook in the T_b interval just below that corresponding to the linear segment on the NRM-TRM diagram. This sample had very good PTRM checks back from a point in the linear segment, but a CRM component larger than the one seen in 6W126. Despite the very different behaviors of these two samples, they yield nearly

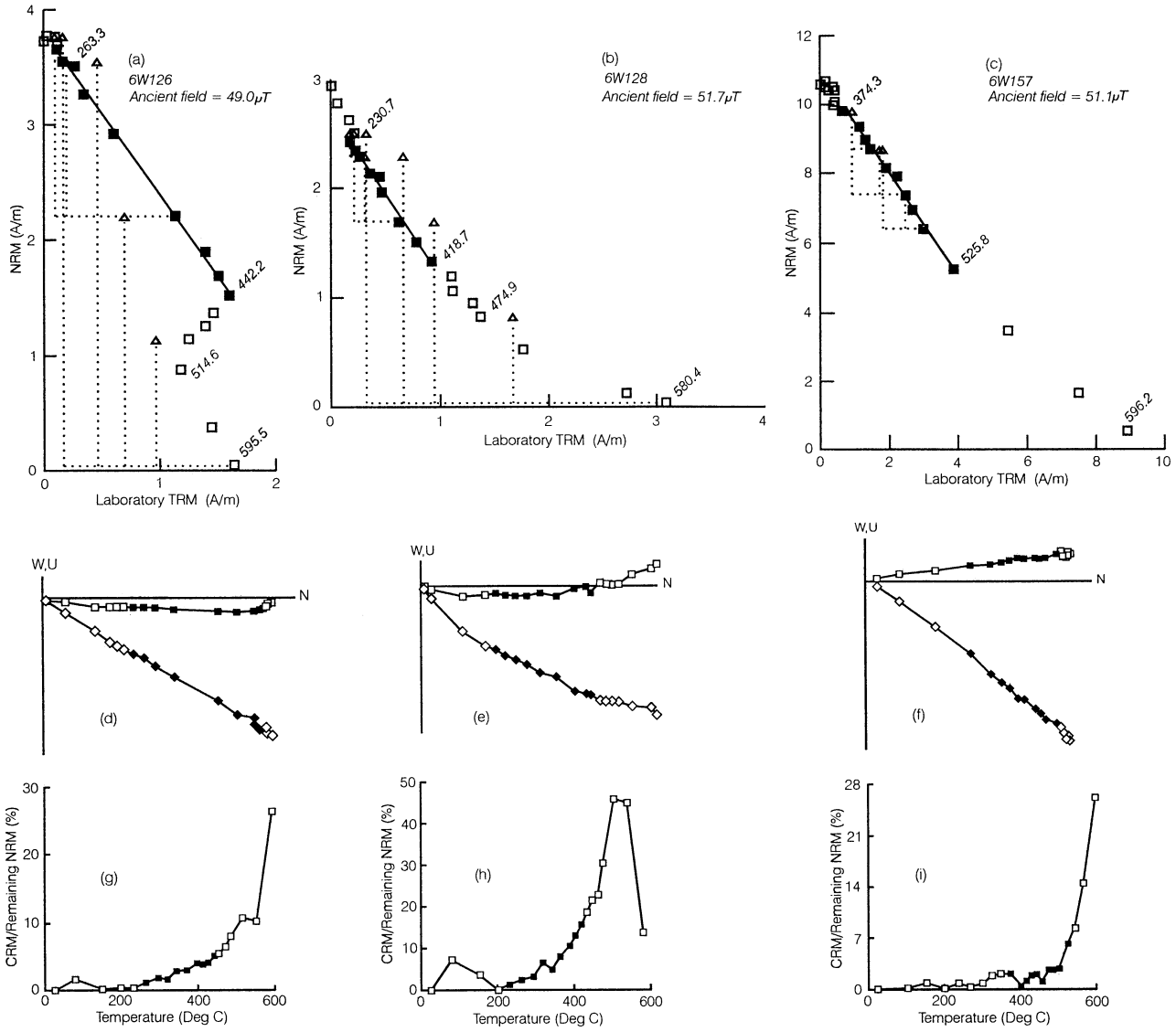

Figure 7. Behavior of three samples exhibiting "hooks" on the NRM-TRM plot. (a-c) NRM-TRM diagrams. (d-f) Vector endpoint diagrams. (g-i) CRM acquisition plots. Some low-temperature PTRM checks for 6W157 have been omitted for clarity. On Figures 7d-7f, squares (diamonds) show the data projected to the horizontal (north-up) plane. Solid symbols on the graphs indicate data from blocking temperature interval used to calculate the sample paleointensity. See Figure 3 for fuller explanations of the plots.

identical paleointensities. Finally, sample 6W157 (from vector group 36, with nearly the same mean paleointensity as vector group 34) has a long linear segment on the NRM-TRM diagram, good PTRM checks, and very low CRM at temperatures below 500°C. Like 6W128, this sample's NRM-TRM diagram shows a small hook at temperatures just below the interval corresponding to the linear NRM-TRM segment.

Of the 64 samples yielding paleointensities, 27 (42%) exhibited relatively straightforward behavior like that of sample 6W144; 7 (11%) had NRM-TRM diagrams like 9Q013 (with a substantial interval of NRM loss but no TRM gain); 15 (23%) had NRM-TRM diagrams like 6W128 and 6W157 (with a small hook before the linear segment); and 10 (16%) had NRM-TRM diagrams like 6W126 (with a large hook after the linear segment). Five samples (8%) had NRM-TRM diagrams showing a small hook before and a larger hook after the linear segment.

Figures 8 through 10 summarize the paleointensity results by showing all NRM-TRM points used to compute the vector group mean paleointensities. Only data from the parts of NRM-TRM diagrams used to compute sample paleointensities are shown, and the axes are scaled so that each vector group mean paleointensity has a slope of -1. Sample paleointensities higher than the vector group mean will have steeper (i.e., more negative) slopes; samples with lower paleointensities will have shallower slopes. These plots show at a glance the number of data defining each vector group mean, their consistency, and the combined fraction of the NRM spanned by the data contributing to the mean. The agreement of sample paleointensities for vector group 35 (on Figure 9), for example, is excellent, while that for vector group 41 (Figure 10) is relatively poor. The scatter is also relatively large for vector group 36 (which is plotted as two subgroups on Figure 10), but we consider the vector group mean paleointensity to be

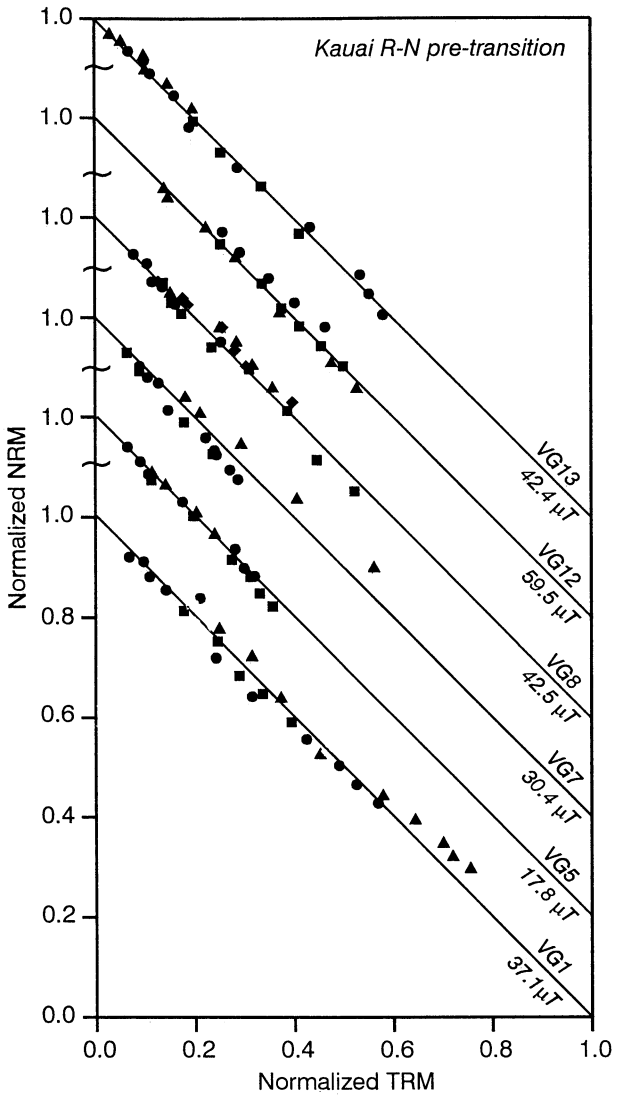

Figure 8. Summary of sample NRM-TRM data used to calculate vector group mean paleointensities for the pretransitional section. Only NRM-TRM pairs used to calculate the sample paleointensity are shown. NRM and TRM scales are arbitrary. Data are scaled to plot with slope -1 if the paleointensity they yield equals their vector group paleointensity (shown with line of slope -1). Sample data are offset to center on the vector group line. Order of symbols in each vector group (lowest sample numbers first): square, circle, triangle, diamond, inverted triangle.

very secure because it based on 10 samples. Of special interest are the vector groups yielding relatively high paleointensities (VG12 in the pretransitional group, Figure 8; VG31 and VG33 in the posttransitional group, Figure 9). Figures 8 and 9 make clear that these paleointensities derive from experimental results that are very typical for this study; the numbers of samples and NRM-TRM points, the within-group precisions, and composite NRM fractions for these three vector groups are all unexceptional.

Table 2 lists the vector group mean paleointensities (i.e., averages of sample paleointensities weighted by quality factor q of *Coe et al.*, [1978]), and Figure 11 gives a sense of how the ancient field intensity varied through time before and after the Kauai R-N transition. The vector groups appear in sequence and equally spaced on the horizontal axis, and so the time element is very approximate. Figure 11 shows that the field grew unusually strong (i.e., well above the mean value for the past 10 m.y. [*Kono and Tanaka,* 1995] both before and after the directional reversal. Notice that these features are defined by the data (solid symbols on Figure 11) which we consider most reliable. As discussed in more detail below, these episodes of high field strength appear to be associated with the recovery of the field from a transitional or transition-like state. It is also apparent on the figure that the field became weak right before both episodes of strong field. The pretransitional flows at Polihale Ridge document an apparently monotonic growth of the field from a low at 17.8 μT to a peak of 59.5 μT. The main directional switch, which occurred well after this episode of strong field, was almost certainly associated with low field strengths (like those recorded by Anahola flows). Following next was a second apparently monotonic rise in field strength that culminated with the highest value (66 μT) recovered in this study and, finally, a decline to near normal field strength. The mean paleointensity was 34.8 μT before the reversal and 47.1 μT after.

4.3 Ancient Field Variation

Table 4 summarizes the variability of the field before and after the Kauai R-N transition. The first four rows describe the

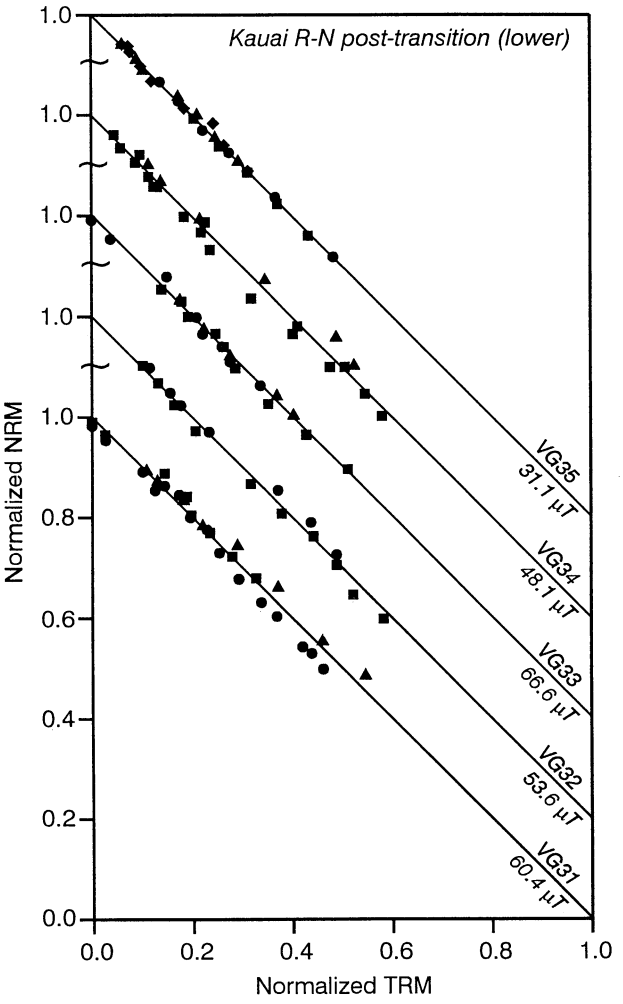

Figure 9. Summary of sample NRM-TRM data used to calculate vector group mean paleointensities for the lower part of the posttransitional section. See Figure 8 for explanation.

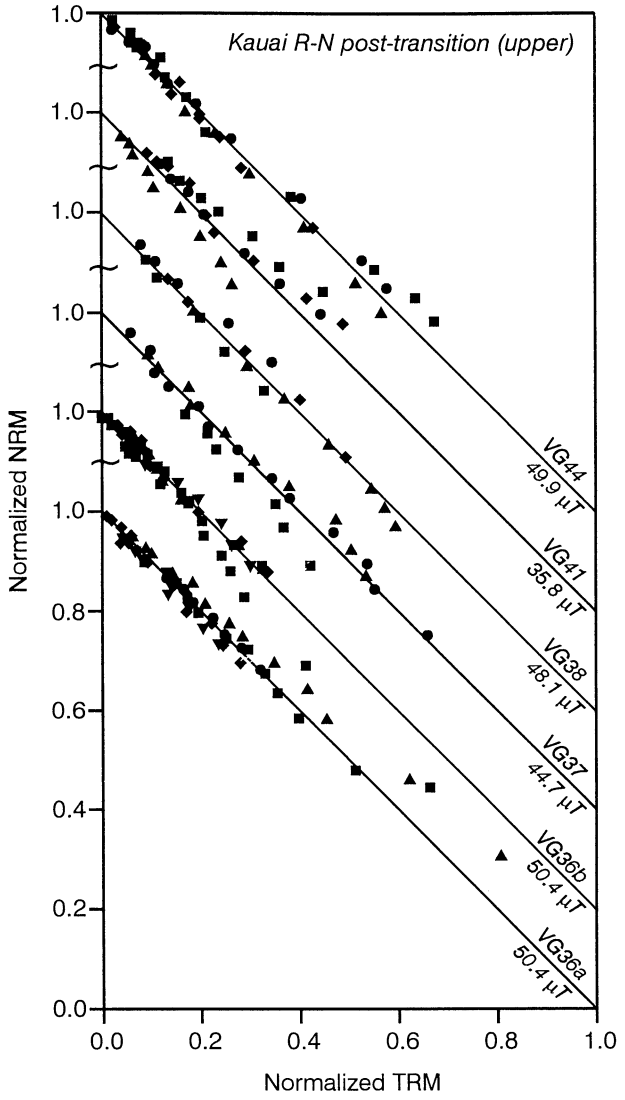

Figure 10. Summary of sample NRM-TRM data used to calculate vector group mean paleointensities for the upper part of the posttransitional section. See Figure 8 for explanation.

directional variation in terms of S, the dispersion of VGPs from the spin axis [*McFadden et al.*, 1988]. For comparison to results from globally distributed volcanic rocks, we calculated an expected value of S by assuming that the Kauai R-N transition occurred at 4 Ma, and then taking a weighted average of values of S at 2.5 Ma (i.e., determined from volcanic rocks younger than 5 m.y. old [*McFadden et al.*, 1988] and at 13.5 Ma (from rocks between 5 and 22 m.y. old [*McFadden et al.*, 1991]). Compared to this expected value (14.2°), S was 31% high before the reversal and 10% low after. In other words, the polarity switch was accompanied by a one-third decrease in the directional variation. There was also a substantial, one-third decrease (from 0.32 to 0.21) in the variation of the field strength (i.e., the normalized standard deviation of the vector mean paleointensities) across the reversal. The net effect of these two changes can be described by calculating the standard deviation of the magnitude of vector differences between the axial dipole vector (assigned a strength equal to the mean paleointensity) and the vector group data. For the Kauai R-N the normalized vector standard deviation (s.d.(V)/PI in Table 4) decreased from 0.49 to 0.29 across the reversal, a decrease of 41%. Keeping in mind that possibility that the vector group data may undersample the true variability, we interpret these substantial differences as evidence that the field was significantly less variable after the Kauai R-N reversal than before.

5. Discussion

In addition to the results from Kauai, Table 4 summarizes the field variability before and after two other reversals recorded in lava sequences. The middle columns summarize field variability before and after the Steens Mountain reversal [*Mankinen et al.*, 1985; *Prévot et al.*, 1985] which occurred ~16 my ago. On the basis of the secular variation (of directions) recorded by the flows, *Mankinen et al.* [1985] estimated that the pretransitional and posttransitional sections spanned 5000 and 3500 years, respectively. Primarily on magnetostratigraphic grounds, *Bogue and Paul* [1993] inferred that the posttransitional section from Ohaiula Ridge preserved several tens of thousands of years of geomagnetic field history, somewhat longer than the comparable interval at Steens Mountain. Because of its proximity to the Ohaiula Ridge section and its similar thickness, it is likely that the Polihale Ridge section spans a comparable amount of time. The mean pretransitional and posttransitional VGPs from the two sections lie reasonably close to the spin axis (all are within twice their α_{95}; three are within α_{95}), an indication that the data do not grossly underestimate the variability of the field.

The rightmost columns of Table 4 correspond to the Matuyama-Brunhes reversal studied in lava flows on La Palma (Canary Islands) by *Valet et al.* [1999]. Like the Kauai R-N record, the flows on La Palma preserve little information on the main directional change but do provide a look at the field before and after the reversal. Four K-Ar ages (ranging from 0.705 Ma to 0.906 Ma) provide control on the time spanned by the pretransitional and posttransitional sections. The pretransitional section appears to span about 160 kyr and the posttransitional about 100 kyr. To make the two parts more comparable to each other and to other data in Table 4, we have calculated statistics on the youngest 100 kyr of the pretransitional record (units 52 through 30). Even with this adjustment, however, the Canary data probably span a much longer interval of time than either the data from Kauai or Steens Mountain. Furthermore, the mean pretransitional and posttransitional VGPs from La Palma lie far (i.e., more than twice their α_{95}) from the spin axis, suggesting that data do not record the full extent of ancient field variation. For both these reasons, conclusions based on the dispersion of the La Palma data are highly uncertain.

As discussed by *Bogue and Paul* [1993], the directional variability of the ancient field after both the Kauai R-N and Steens Mountain reversals was close to that expected from model G of *McFadden et al.* [1988, 1991]. The comparison can now be extended to include the pretransitional directional variation, which in both cases is significantly greater (31% for Kauai and 27% for Steens Mountain) than predicted by model G. The variation of directional dispersion is therefore the same for both reversals, decreasing substantially across the polarity switch. The results from La Palma, however, are quite different, with directional variation increasing by 60% across the reversal to become 41% higher than predicted by model G. As discussed above, the La Palma data are problematic in several ways. Nevertheless, it would be very bad luck if the 39 units from La Palma sampled the ancient field variation so poorly that what

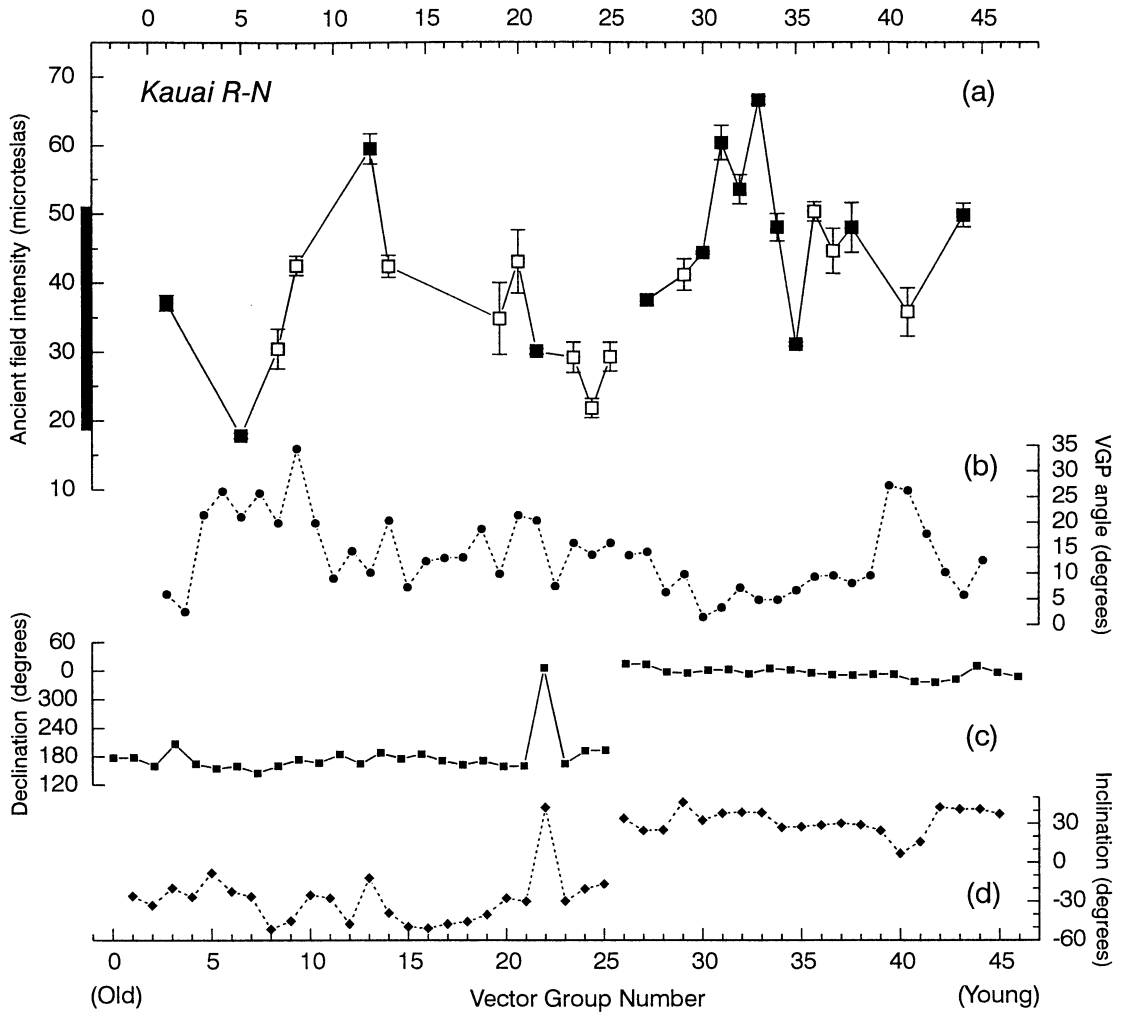

Figure 11. (a) Ancient field intensity, (b) VGP angle, (c) declination, and (d) inclination versus vector group number. The time sequence runs from left to right, but the horizontal scale is arbitrary and not uniformly spaced in time. In Figure 11a, solid symbols denote vector groups for which all constituent sample paleointensities are within 10% of the vector group mean and at least half have q>2.5; these data are considered the most reliable. Solid bar on the left vertical axes shows the range of field strengths (at the latitude of the Hawaiian hotspot) corresponding to paleomagnetically determined post-10 Ma dipole average (± standard deviation) of *Kono and Tanaka* [1995]. The present-day field in Kauai is 36 μT. A preliminary version of this plot showing the posttransitional results appeared in the work by *Bogue and Paul* [1993]. Figure 11b shows the angle between the VGP and Earth's spin axis (South Pole for vector groups 1 through 25; North Pole for vector groups 26 through 35). As can be seen in Figures 11c and 11d, the main directional switch occurs between vector groups 25 and 26.

appears to be a large increase is actually a decrease in dispersion. So, in spite of the excellent agreement between the Kauai and Steens Mountain records, the evidence from all three records suggests that a decrease in directional variation is not a systematic feature of reversals.

Prévot et al. [1985] noticed that the paleointensity was more variable after the Steens Mountain reversal than before and speculated that this difference might reflect the instability of the newly established dipole field. The change in variability is best expressed in Table 4 as the standard deviation of vector mean paleointensity normalized by the corresponding mean paleointensity (s.d.(PI)/PI). Across the Steens Mountain reversal, the s.d.(PI)/PI went from 0.27 to 0.43, an increase of almost 60%. The Kauai record, however, show the opposite; the s.d.(PI)/PI decreases by about a third. A similar change is evident in the La Palma data, although, as discussed above, they represent a longer time interval and apparently undersample the variation. Nevertheless, if the Kauai and La Palma data are interpreted in same fashion as by *Prévot et al.* [1985[, one would conclude that the newly established dipole was more stable than it was right before the reversal. Together, the Steens Mountain and Kauai data show that that large changes in the variability of field strength (one third or more) can occur across polarity transitions but that both increases and decreases are possible.

The final rows in Table 4 show before and after values of s.d.(V), a statistic that expresses the combined effect of changes in directional and intensity variation. For Kauai, where both the direction and intensity became less variable after the reversal, the normalized s.d.(V)(i.e., s.d.(V)/PI) showed a substantial (41%) decrease across the polarity transition. Taken alone, this evidence might suggest that the process of reversal significantly suppresses field change in the posttransitional interval. At Steens Mountain,

Table 4. Field Variation Before and After Three Reversals[a]

	Kauai R-N		Steens Mountain		La Palma, selected	
	Pre	Post	Pre	Post	Pre	Post
N	12	13	10	13	16	13
S, deg	18.6	12.9	25.0	18.8	12.6	20.3
S/S_g	1.30	0.90	1.27	0.95	0.88	1.41
S/S_g [b]	1	0.69	1	0.75	1	1.60
Mean PI, μT	34.8	47.1	31.5	46.7	33.2	47.0
Mean PI [b]	1	1.35	1	1.48	1	1.42
s.d.(PI), μT	11.1	9.8	8.5	20.1	11.6	11.9
s.d.(PI)/PI [b]	1	0.66	1	1.59	1	0.71
s.d.(V), μT	16.9	13.4	13.0	22.6	14.4	20.3
s.d.(V) [b]	1	0.79	1	1.74	1	1.41
s.d.(V)/PI [b]	1	0.59	1	1.17	1	1.00

[a] *N*, number of vector groups used to calculate statistics; *S*, angular standard deviation of ancient field directions from spin axis; S_g, prediction of *S* from model G of *McFadden et al.* [1988]; PI, paleointensity; s.d.(PI); standard deviation of paleointensities; s.d.(V); vector standard deviation (see text).

[b] Values divided by the corresponding pre-transitional value.

however, the changes in directional and paleointensity variation were of opposite sign and so tended to cancel, leading to only a small (-12%) change in the normalized s.d.(V). Once again, the available data provide no support to the idea that this kind of change (or lack of it) is systematic. It is also interesting that the absolute magnitude of s.d.(V) shows a very large increase across the Steens Mountain reversal. This observation is not consistent with suggestions [*Mary and Courtillot*, 1993; *Camps and Prévot*, 1996] that the nondipole field remains largely unchanged through the reversal process.

The only feature clearly shared by all three records is that the field became unusually strong shortly after reversing. This aspect of the Kauai and Steens Mountain records was discussed by *Bogue and Paul* [1983] and was discussed for the La Palma record by *Valet et al.* [1999]. Bogue and Paul [1983] interpreted the high field strength as evidence that the geodynamo remains in an unusual state for many tens of thousands of years following a polarity reversal. *McFadden and Merrill* [1993] provided the basis for this interpretation by their analysis of the geomagnetic timescale. They inferred from the absence of short polarity events over the past 160 m.y. that some property (e.g., magnetic field configuration or state of the core fluid motion) acted to inhibit reversals in the immediate posttransitional interval. *Gubbins* [1999] has implicitly suggested a mechanism for this inhibition by speculating on the role that the inner core plays in reversals. In his model, the immediate posttransitional interval would always be characterized by the fields of both the inner and outer cores having the same sign. In such a state, polarity reversal would be inhibited for as long as it takes field of opposite sign to permeate the inner core, several thousand years at least. The paleomagnetic data from Kauai, Steens Mountain, and La Palma suggest that a strong poloidal field may be another manifestation of this state of the geodynamo.

It is intriguing that the highest field strength seen in the pretransitional record from Kauai follows a substantial swing of the VGP toward South America. *Hoffman* [1992] has argued that the VGP positions near the southern tip of South America may represent a briefly stable, intermediate field configuration that has recurred during polarity transitions for the last 20 m.y. If so, then it is possible that the movement of the VGP toward South America right before the Kauai R-N reversal resulted from the geodynamo approaching this metastable intermediate state as part of an unsuccessful reversal attempt. The low paleointensity (17.8 μT) of VG5 (on the swing toward South America) supports the idea that this swing represents reversal-like behavior even though the VGP returns to high southerly latitudes before the main polarity switch. The high field strength (59.5 μT) of VG12, the high-latitude VGP that marks the end of the swing, anticipates the strong field that appears just after the main transition itself. This observation suggests that strong field characterizes the geodynamo upon its return from intermediate states, polarity reversed or not.

The posttransitional increase in field intensity seen in the record from Kauai appears to be relatively short-lived. The entire feature occurs in the first 17 m (i.e., from the R-N horizon up through flow OR9) of a normally magnetized section that is at least 300 m thick. Judging by stratigraphic thickness alone, the episode of high field strength occurred within the first 6% of the normal polarity interval following the reversal, suggesting a duration of less than 10 kyr. Notice that high field strength associated with a transient, reversal-related phenomenon differs from the strong, postreversal field of the controversial "sawtooth" hypothesis [*Valet and Meynadier*, 1993]. According to sawtooth model, field intensity becomes high immediately following a geomagnetic reversal (as is seen in these data) but then declines almost linearly over the entire interval of stable polarity. Clearly, high posttransitional field intensity in the sawtooth model is not associated with a short-lived, postreversal state of the geodynamo but rather an initial condition that subsequently evolves over a timescale 10 times as long (typically several hundreds of thousands of years). Another prediction of the sawtooth hypothesis, low field intensity that greatly proceeds the directional transition, is also not apparent in the data from Kauai.

6. Summary of Conclusions

On the basis of a comparison of three paleomagnetic records from lava flows of the field shortly before and after polarity reversal, it appears that the variability of the pretransitional and posttransitional fields can be very different. The two best data sets (Kauai R-N and Steens Mountain) show a remarkably similar decrease in directional dispersion across the polarity reversal, and all three records provide evidence that the geodynamo produces unusually strong magnetic field after returning from its intermediate state. The data from Kauai show in addition that strong field follows an abortive reversal attempt in the pretransitional interval. Strong posttransitional field intensity appears to be a transient phenomenon, possibly related to conditions in the geodynamo that inhibit reversals for several tens of thousands of years following a reversal. The data do not lend support to the sawtooth model in which high posttransitional intensity is related to chron-scale evolution of the geodynamo rather than to short-lived phenomena associated with the polarity reversal itself.

Appendix A: Detailed Description of the Paleointensity Experiment

A1. Experimental Apparatus

The furnace used for the paleointensity experiments is a ceramic cylinder (10 cm diameter) with noninductive nichrome windings. Six chromel-constantan thermocouples (connected to a

commercial interface board) measure the sample temperatures during the heatings. The thermocouples are cemented in the center of ceramic cylinders the same size as the paleomagnetic specimens and positioned along the length of the sample carrier. By regulating the oven power voltage and (in later experiments) adjusting the heating rate by cycling the oven power (via microcomputer-controlled relays), the approach to the set temperatures is slow, <1°C/min. Maximum temperatures measured by the thermocouples are interpolated to sample positions using cubic splines. Temperature differences between samples at the ends and the center of the carrier were of the order of 5%. On average, the temperatures reached by a specimen in the paired field-on and field-off heatings differed by less than a degree. In a few instances, however, temperature differences up to 4°C occurred for samples near the ends of the sample carrier where the temperature gradients were largest. As described below, we made small corrections to the NRM-TRM to compensate for temperature mismatches. Samples usually went from room temperature to the set temperature in about an hour and took 4 to 5 times as long to cool.

Coaxial with the furnace is a 19-cm-diameter solenoid which can be switched on and off by the microcomputer. The solenoid and furnace sit inside a two-layer cylindrical shield made of a high permeability alloy ("hipernom"), and the entire assembly is oriented 90° to the ambient magnetic field. With the solenoid off, the fields at sample positions within the furnace were <30 nT. We measured these low fields and calibrated the solenoid with a commercial (APS model 250) three-axis fluxgate magnetometer.

The sample carrier, which can hold up to 22 specimens, is a titanium frame that slides into the furnace along a rail fashioned from a split 2.54-cm-diameter titanium tube. The samples were standard 10 cm^3 paleomagnetic core sections. In the first two of the six batches run, the samples were aligned on the sample carrier to that their cylindrical (z) axes were parallel to the field produced by the solenoid. For the last four batches the samples were placed on the sample frame so that their z axes were perpendicular to the laboratory field. Each sample had a small groove sawn into one end that fit onto a 2 mm titanium rod secured to the sample carrier frame. The grooves were oriented so that each sample's NRM was aligned 90° to the field produced by solenoid.

A2. Sample Selection

We chose samples whose (undemagnetized) NRMs were close to their respective flow-mean directions (which derived from AF demagnetization experiments). By this procedure, we hoped to select samples without substantial secondary components of magnetization. For these samples we determined how their initial susceptibility (χ) varied with temperature (from -150°C to 700°C, in air). This test helped us identify those samples that were especially prone to alteration in the paleointensity experiment (e.g., those that had only partially oxidized during original cooling). We avoided samples whose χ-T curve underwent large changes upon heating (especially the disappearance of a broad maximum centered near 300°C). Once promising samples were identified, we subjected the deepest, least-weathered specimen (previously unused) from the core to a 2-week storage test in the earth's field, looking for samples would acquire a viscous remanent magnetization <5% their NRM. The final check enabled us to avoid samples with significant populations of large, magnetically soft grains.

A3. Analysis of NRM-TRM Data

We used the procedure below to interpret the results of the double-heating experiments:

1. We picked an "ideal" NRM direction for each sample by inspecting its orthogonal vector demagnetization diagram, looking for a direction that was not contaminated by either secondary components (e.g., Brunhes age VRM) or a component in the laboratory field direction. Because we used only samples that appeared to be free of secondary components, this ideal direction was often just the original NRM.

2. In order to determine how each sample was oriented with respect to the induced field in the furnace, we did a final field-on heating to a temperature well above the T_c of magnetite. The remanence produced by this heating served as an ideal PTRM direction. The ideal NRM and ideal PTRM directions define an ideal plane onto which all the remanence directions for each sample were projected.

3. The remanence measured after the field-off step at T_n was projected onto the ideal plane and then decomposed into components along the ideal NRM and ideal PTRM directions. We use the magnitude of the former component as the best estimate of the NRM_n (i.e., the NRM remaining at after heating to T_n) and take the magnitude of the latter component as a measure of CRM_n (i.e., all CRM in the laboratory field direction with $T_h > T_n$).

4. To find the $PTRM_n$, we projected and decomposed the remanence measured after each field-on step at T_n just like described above for the field-off step. We then vectorially subtracted the projected NRM from the field-off step, which includes both the NRM component remaining plus any CRM in the laboratory field directions acquired so far in the experiment. Finally, we made a correction to this resultant ($PTRM_n$) for any temperature mismatch between the field-on and field-off heatings using a factor derived from rate of NRM loss over the next lowest-temperature interval. As described above, the temperature mismatches were small, and consequently, the PTRM corrections averaged <1% (and never exceeded 5% for NRM-TRM points used to infer a paleointensity).

5. We examined five criteria when deciding to accept or reject a paleointensity result from a sample. The first two were whether a linear segment on the NRM-TRM diagram could be identified (by eye) and whether PTRM checks over the relevant temperature interval showed that TRM capacity had not changed significantly. For samples meeting these first two criteria, we then made sure that for all points the apparent CRM fraction (i.e., the apparent CRM divided by the ideal NRM at that heating step) was low. As can be seen in Table 3, the average CRM fraction at the highest temperature NRM-TRM point was ~10%, and for only one sample did the value exceed 17%. For several samples the presence of substantial apparent CRM forced us to exclude one or more high temperature NRM-TRM points from linear segments that otherwise looked acceptable. Finally, we calculated the various measures of experimental quality proposed by *Coe et al.* [1978]. The average value of f (the fraction of the NRM spanned by the linear segment from which the paleointensity is derived) was 33.6%; the lowest f we accepted was 12.4%. The average value of q ("quality factor") was 3.9; the lowest value we accepted was 0.8. Of the 128 samples that met the selection criteria described above, 64 (50%) yielded acceptable results.

Acknowledgments. The "we" used throughout this paper includes the 9 Occidental College students who played key roles in the research. Hugi Olaffsson assisted with the sample

collection on Kauai. Hugi and Kenji Shintaku performed the initial directional measurements on the samples. Kenji, Jeff Witter, and Greg Wells helped design and build the paleointensity apparatus. Lance King, Kirsten Menking, Doug Reeves, Hilary Paul, and Kindra Loomis worked on the paleointensity experiments and associated rock magnetic measurements. Thanks to Joe Kirschvink for allowing use of his AF demagnetizer. Helpful reviews were provided by Jean-Pierre Valet, Heinrich Soffel, and the AE. This research was supported by grants from the National Science Foundation and the Research Corporation.

References

Arai, Y., Secular variation in the intensity of the past geomagnetic field, MS thesis, Univ. of Tokyo, Tokyo, 1963.

Bogue, S. W., Behavior of the geomagnetic field during successive reversals recorded in basalts on Kauai, Hawaii, Ph.D. thesis, Univ. of Calif., Santa Cruz, 1982.

Bogue, S. W., and R. S. Coe, Successive palaeomagnetic reversal records from Kauai, *Nature, 295*, 399-401, 1982.

Bogue, S. W., and R. S. Coe, Transitional paleointensities from Kauai, Hawaii, and geomagnetic reversal models, *J. Geophys. Res.*, *89*, 10,341-10,354, 1984.

Bogue, S. W., and R. T. Merrill, The character of the field during geomagnetic reversals, *Annu. Rev. Earth Planet. Sci.*, *20*, 181-219, 1992.

Bogue, S. W., and H. A. Paul, Distinctive field behavior following geomagnetic reversals, *Geophys. Res. Lett.*, *20*, 2399-2402, 1993.

Camps, P., and M. Prévot, A statistical model of the fluctuations in the geomagnetic field from paleosecular variation to reversal, *Science*, *273*, 776-779, 1996.

Cande, S. C., and D. V. Kent, Revised calibration of the geomagnetic polarity timescale for the Late Cretaceous and Cenozoic, *J. Geophys. Res.*, *100*, 6093-6095, 1995.

Clement, B. M., Geographical distribution of transitional VGPs: Evidence for non-zonal equatorial symmetry during the Matuyama-Brunhes geomagnetic reversal, *Earth Planet. Sci. Lett.*, *104*, 48-58, 1991.

Coe, R. S., Paleo-intensities of the earth's magnetic field determined from Tertiary and Quaternary rocks, *J. Geophys. Res.*, *72*, 3247-3262, 1967.

Coe, R. S., C. S. Grommé, and E. A. Mankinen, Geomagnetic paleointensities from radiocarbon-dated lava flows on Hawaii and the question of the Pacific nondipole low, *J. Geophys. Res.*, *83*, 1740-1756, 1978.

Engebretson, D. C., A. Cox, and R. Gordon, Relative motions between oceanic and continental plates in the Pacific basin, *Spec. Pap. Geol. Soc. Am.*, *206*, 1-59, 1985.

Fisher, R. A., Dispersion on a sphere, *Proc. R. Soc. London Ser. A*, *217*, 295-305, 1953.

Glatzmaier, G. A., and P. H. Roberts, A three-dimensional self-consistent computer simulation of a geomagnetic field reversal, *Nature*, *377*, 203-209, 1995.

Glatzmaier, G. A., R. S. Coe, L. Hongre, and P. H. Roberts, The role of the Earth's mantle in controlling the frequency of geomagnetic reversals, *Nature*, *401*, 885-890, 1999.

Gubbins, D., The distinction between geomagnetic excursions and reversals, *Geophys. J. Int.*, *137*, F1-F3, 1999.

Hoffman, K. A., Dipolar reversal states of the geomagnetic field and core-mantle dynamics, *Nature*, *359*, 789-794, 1992.

Holcomb, R. T., D. Champion, and M. McWilliams, Dating recent Hawaiian lava flows using secular variation, *Geol. Soc. Am. Bull.*, *97*, 829-839, 1986.

Holcomb, R. T., P. W. Reiners, B. K. Nelson, and N. E. Sawyer, Evidence for two shield volcanoes exposed on the island of Kauai, Hawaii, *Geology*, *25*, 811-814, 1997.

Kono, M., and H. Tanaka, Intensity of the geomagnetic field in geological time: A statistical study, in *The Earth's Central Part: Its structure and dynamics*, edited by T. Yukutake, pp. 75-94, Terrapub, Tokyo, 1995.

Kosterov, A. A., and M. Prévot, Possible mechanisms causing failure of Thellier palaeointensity experiments in some basalts, *Geophys. J. Int.*, *134*, 554-572, 1998.

Laj, C., A. Mazaud, R. Weeks, M. Fuller, and E. Herrero-Bervera, Geomagnetic reversal paths, *Nature*, *351*, 447, 1991.

Langenheim, V. A. M., and D. A. Clague, The Hawaiian-Emperor volcanic chain, part II., Stratigraphic framework of volcanic rocks of the Hawaiian Islands, *U.S. Geol. Surv. Prof. Pap.*, *1350*, 55-84, 1987.

MacDonald, G. A., D. A. Davis, and D. C. Cox, Geology and ground-water resources of the island of Kauai, Hawaii, *Bull. 13 Hawaii Div. of Hydrogr.*, 1960.

Mankinen, E. A., M. Prévot, C. S. Grommé, and R. S. Coe, The Steens Mountain (Oregon) geomagnetic polarity transition, 1,. Directional history, duration of episodes, and rock magnetism, *J. Geophys. Res.*, *90*, 10,393-10,416, 1985.

Mary, C., and V. Courtillot, A three-dimensional representation of geomagnetic reversal records, *J. Geophys. Res.*, *98*, 22,461-22,475, 1993.

McFadden, P. L., and R. T. Merrill, Inhibition and geomagnetic field reversals, *J. Geophys. Res.*, *98*, 6189-6199, 1993.

McFadden, P. L., R. T. Merrill, and M. W. McElhinny, Dipole/quadrupole family modeling of paleosecular variation, *J. Geophys. Res.*, *93*, 11,583-11,588, 1988.

McFadden, P. L., R. T. Merrill, M. W. McElhinny, and S. Lee, Reversals of the Earth's magnetic field and temporal variations of the dynamo families, *J. Geophys. Res.*, *96*, 3923-3933, 1991.

Merrill, R. T., A magnetic reversal record (news and views), *Nature*, *389*, 678-679, 1997.

Merrill, R. T., and P. L. McFadden, Geomagnetic polarity transitions, *Rev. Geophys.*, *37*, 201-226, 1999.

Prévot, M., and P. Camps, Absence of preferred longitude sectors for poles from volcanic records of geomagnetic reversals, *Nature*, *366*, 53-57, 1993.

Prévot, M., E. A. Mankinen, S. Grommé, and A. Lecaille, High paleointensities of the geomagnetic field from thermomagnetic studies on rift-valley pillow basalts from the Mid-Atlantic ridge, *J. Geophys. Res.*, *88*, 2316-2326, 1983.

Prévot, M., E. A. Mankinen, R. S. Coe, and C. S. Grommé, The Steens Mountain (Oregon) geomagnetic polarity transition, 2, Field intensity variations and discussion of reversal models, *J. Geophys. Res.*, *90*, 10,417-10,488, 1985.

Tanaka, H., M. Kono, and H. Uchimura, Some global features of palaeointensity in geological time, *Geophys. J. Int.*, *120*, 97-102, 1995.

Thellier, E., and O. Thellier, Sur l'intensite du champ magnetique terrestre dans le passe historique et geologique, *Ann. Geophys.*, *15*, 285-376, 1959.

Tric, E., C. Laj, C. Jehanno, J.-P. Valet, C. Kissel, A. Mazaud, and S. Iaccarino, High resolution record of the Upper Olduvai transition from Po valley (Italy) sediments: Support for dipolar transition geometry?, *Phys. Earth Planet. Inter.*, *65*, 319-336, 1991.

Valet, J.-P., and L. Meynadier, Geomagnetic field intensity and reversals during the past four million years, *Nature*, *366*, 234-238, 1993.

Valet, J.-P., J. Brassart, X. Quidelleur, V. Soler, P.-Y. Gillot, and L. Hongre, Paleointensity variations across the last geomagnetic reversal at La Palma, Canary Islands, Spain, *J. Geophys. Res.*, *104*, 7577-7598, 1999.

S. Bogue, Department of Geology, Occidental College, 1600 Campus Road, Los Angeles, CA 90041. (bogue@oxy.edu)

(Received August 4, 1999; revised July 21, 2000;
accepted August 21, 2000.)